Available online at www.sciencedirect.com
ScienceDirect
Catalysis Today 133–135 (2008) 357–366
CATALYSIS TODAY
www.elsevier.com/locate/cattod

CO_2 reforming of methane over Ni/Mg/Al/Ce mixed oxides

Carlos Enrique Daza [a], Jaime Gallego [b], Jorge Andrés Moreno [b], Fanor Mondragón [b], Sonia Moreno [a], Rafael Molina [a,*]

[a] *Estado Sólido y Catálisis Ambiental, Departamento de Química, Facultad de Ciencias, Universidad Nacional de Colombia, AK 30, No. 45-03, Bogotá, Colombia*

[b] *Química de Recursos Energéticos y Medio Ambiente, Instituto de Química, Universidad de Antioquia, P.O. Box A.A. 1226, Medellín, Colombia*

Available online 19 February 2008

Abstract

Ni/Mg/Al/Ce mixed oxides were synthesized by thermal decomposition of layered double hydroxide-type compounds, which were obtained by the coprecipitation method at constant pH. The effect of the Ni^{2+} and Ce^{3+} incorporation methods in the hydrotalcite-type structure was studied. The solids were characterized using chemical analysis by X-ray fluorescence (XRF), X-ray diffraction (XRD), thermogravimetric analysis (TGA–DTG), diffuse reflectance infrared spectroscopy (DRIFT), temperature programmed reduction (TPR-H_2), BET surface areas and scanning electron microscopy (SEM). The methane reforming reaction was carried out at 700 °C. The results demonstrate the formation of solids with mixed crystalline phases of NiO–MgO (periclase) type and CeO_2 (fluorite) as well as other types of reducible species. Catalysts with CH_4 conversions of 50–80%, CO_2 conversions of 80–90%, CO selectivities of 20–40% and H_2 of 18–30% and high stability under the reaction conditions were obtained. Cerium promotes the catalytic activity of this type of solids. The catalyst with the best activity was obtained by coprecipitation of Ni^{2+}, Mg^{2+}, Al^{3+} and Ce^{3+}.

Keywords: Hydrotalcites; Cerium; CO_2 reforming of methane

1. Introduction

For several decades, there has been a remarkable worldwide interest in developing processes to transform natural gas into products with a greater added value in order to obtain economic benefits. Among the alternatives for increasing natural gas value, the transformation of methane, its major component, into a synthesis gas ($CO + H_2$) stands out, due to its vital importance in chemical industry as it is used in the production of several synthetic fuels [1–3]. One of the methods to obtain the synthesis gas is by the CO_2 reforming of methane. This procedure has captured significant attention due to different aspects: (i) H_2/CO mole ratios approaching 1 are obtained, which are adequate in the production of oxygenated compounds through the Fischer–Tropsch process; (ii) raw materials are related to the greenhouse effect, and consequently this process may have important environmental implications, particularly when used in the conversion of natural gas with large CO_2 contents; (iii) the reaction, due to its endothermic and reversible nature, can be used in the recovery and storage of energy [2,3].

The reaction is usually catalyzed by nickel [2,4–10] or noble metals [11–13], the former being favoured due to its low cost and availability. However, catalysts are deactivated due to the formation and accumulation of coke on their surface during the reaction, especially those containing nickel [1,2]. High dispersion of active metals and the use of basic or redox precursors reduce the deposition of coke [2,3]. Cerium, known as an oxygen accumulator [14,15], acts as promoter thus yielding beneficial effects in the nickel dispersion and decrease of coking in nickel catalysts [16–18].

Among the catalytic systems studied, those derived from layered double hydroxide (LDH)-type precursors have shown a better catalytic behaviour than those obtained by conventional techniques [19,20]. Traditionally, LDH are synthesized by the coprecipitation at constant pH of Mg^{2+} and Al^{3+}, and of guest ions like Ni^{2+} which perform isomorphic substitution in the brucitic layer of the LDH structure [20,21]. The thermal decomposition of these precursors generates the formation of mixed oxides with homogeneous interdispersion of the constituting metals and strong basic character [22–25]. An

* Corresponding author. Fax: +57 1 316 5220.
E-mail address: ramolinag@unal.edu.co (R. Molina).

0920-5861/$ – see front matter © 2007 Elsevier B.V. All rights reserved.
doi:10.1016/j.cattod.2007.12.081

alternative LDH synthesis technique has been recently reported, whereby metals can be included as anionic complex with $EDTA^{4-}$ in the interlayer space of the LDH via coprecipitation and/or reconstruction [22–26]. Likewise, this technique has been used in the inclusion of two metals by means of the reconstruction method for the production of bimetallic catalysts [24].

However, in spite of the versatility of synthesis methods, the preparation of mixed oxides containing redox metals like cerium starting from LDH-type precursors to obtain promoted nickel catalysts has not been reported. This paper reports the characterization and catalytic activity/selectivity in the reaction of CO_2 reforming of methane within the framework of the study of mixed oxides synthesis methods starting from LDH involving Ni^{2+} and Ce^{3+} ions.

2. Experimental

2.1. Catalysts preparation

Nitrates of the corresponding metals were dissolved in 500 mL of deionised water. The metal solution was added by dripping on 500 mL of a Na_2CO_3 (150 mmol) solution at 60 °C and pH 10.5. The suspension was aged by agitation for 1 h at 60 °C, and then without agitation for 18 h at 60 °C. The solid, previously washed with deionised water, and dried for 24 h at 60 °C (HT series), was calcined at 500 °C/16 h to obtain the mixed solid (OM series) [23,26]. In the case of the procedure with metal–$EDTA^{4-}$ complexes, coprecipitation was performed on the complex previously synthesized by means of methodologies already reported [24,26]. Table 1 shows the molar quantities used in the synthesis of mixed oxides through the coprecipitation methodology.

2.2. Characterization

Chemical analysis of the solids was carried out by means of the X-ray fluorescence technique with a PHILLIPS MAGIX PRO PW2440 equipment. X-ray diffractograms in powder were taken with a PHILLIPS PW1710 equipment using a copper anode. The particle sizes were calculated using the Scherrer equation. Thermogravimetric analyses were carried out by means of TA-INSTRUMENT 2950 equipment, with ±0.001 mg accuracy, in a N_2 atmosphere, at 100 mL/min and a heating ramp of 10 °C/min. DRIFT spectra were taken by means of a MAGNA IR 560 NICOLET equipment, under environmental conditions.

Table 1
Quantities used in the synthesis of mixed solids by means of the coprecipitation method

Solid	Mg^{2+} (mmol)	Al^{3+} (mmol)	Ni^{2+} (mmol)	Ce^{3+} (mmol)
OM1	100	50	50	–
OM2	100	45	50	5
OM3	150	45	250[a]	5
OM4	100	50	50	50[a]

[a] Used as complexes with $EDTA^{4-}$.

TPR-H_2 profiles were taken by means of a CHEMBET 3000 (QUANTACHROME) equipment fitted with a thermal conductivity detector, following already reported methodologies. The samples (<250 μm) were previously degasified at 400 °C for 1 h in Ar and reduced with a heating ramp of 10 °C/min using 10% (v/v) H_2/Ar at 0.38 mL/s. Tests were carried out under conditions granting results which are free from the effects of operation variables in the form and at maximal temperature (T_M) for reduction profiles [27,28].

Pre-treatments on catalysts were carried out at 700 °C for 1 h, with a flow of pure H_2 at 40 mL/min, with a heating ramp of 10 °C/min and then cooled down with an Ar flow at 40 mL/min. TPR-H_2 tests were performed under the conditions previously described.

BET surface areas were measured by nitrogen adsorption at 77 K using a Micromeritics ASAP 2000 apparatus. Scanning electron microscopy (SEM) analyses were performed by means of a FEI QUANTA 200 equipment, which features an energy dispersive X-ray (EDX) microanalysis system.

2.3. Catalytic evaluation

Catalytic tests were performed using 50 mg of the mixed oxide in powder (<250 μm), details of the procedure have been previously reported [4,5]. The temperature was increased up to 700 °C at 4 °C/min. The samples were reduced in situ with pure H_2 at 40 mL/min for 1 h. The reactor was fed with CH_4/CO_2/He in the ratio 20/20/60 for a total flow of 100 mL/min and a spatial velocity of 48,000 mL/(g h). The reaction products were analyzed with an online quadrupole mass spectrometer.

3. Results

Given the lamellar-type structure of LDH, simultaneous coprecipitation was performed in order to obtain the formation of compound brucitic layers for the metals employed. Coprecipitation in the presence of Ce^{3+} ions was carried out in order to obtain isomorphic substitution by Al^{3+} ions. On the other hand, coprecipitation by means of metals complexed with $EDTA^{4-}$ was performed in order to manage the inclusion of these metals in an anionic way in the interlamellar space of the LDH structure [24,26].

Table 2 shows the chemical analysis of mixed oxides performed by X-ray fluorescence. The results confirm the chemical modification and indicate that Ni and Ce compositions depend on the inclusion method used. It can be observed that the solid synthesized in the presence of complex

Table 2
Chemical analysis of mixed oxides by X-ray fluorescence

Solid	Al_2O_3 (%)	MgO (%)	NiO (%)	CeO_2 (%)	Ni/Mg	Mg/Al	Ce/Ni	Ce/Al
OM1	19.88	30.07	49.31	–	0.88	1.91	–	–
OM2	18.70	30.57	48.03	14.90	0.85	2.07	0.13	0.24
OM3	23.68	67.50	5.83	2.81	0.05	3.61	0.21	0.04
OM4	18.26	38.98	17.97	34.83	0.25	2.70	0.84	0.57

$[Ni(EDTA)]^{2-}$ (OM3) shows the lowest NiO content, indicating a low inclusion of nickel achieved through this method. On the other hand, the OM4 solid is the one showing the highest CeO_2 content. In general, results are coherent with the nominal quantities used in each one of the synthesis methods.

3.1. X-ray diffraction analysis

Fig. 1 shows the X-ray diffractograms of LDH precursors (HT series). Diffractograms of the solids synthesized in the presence of Ce^{3+} (HT2–HT4) show the signals of the carbonated phase of hydrotalcite [19], and signals characterizing the fluorite structure of CeO_2. A lower crystallinity of the hydrotalcite phase is observed in these solids as compared with Ni/Mg/Al hydrotalcite (HT1), expressed as lower intensities in diffraction lines.

On the other hand, it is evident that the different methods for the inclusion of metals cause the formation of hydrotalcites with different compositions and crystallinity. Table 3 presents the crystallographic parameters of hydrotalcites obtained in this work calculated according to procedures suggested in literature [19]. In the first place, we can observe that crystallographic parameter *c*, in the case of solids prepared by coprecipitation with complexing metals did not vary with respect to the solids obtained by coprecipitation with CO_3^{2-}, indicating that in all cases a carbonated phase was obtained [19]. This result indicates that there was no inclusion of complexing metals in the interlayer space of the hydrotalcite structure, which suggests that the inclusion of metals by this method was performed in the surface of the solid, generating a metal coating, which goes in line with what other authors have reported [23].

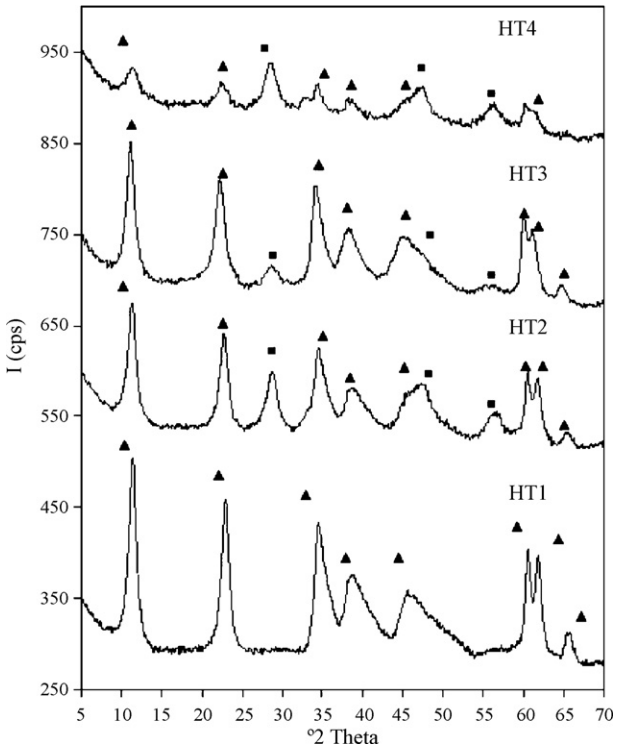

Fig. 1. XRD for the hydrotalcites: (▲) hydrotalcite and (■) CeO_2.

Table 3
Crystallographic parameters of layered double hydroxides

Solid	*c* (nm)	*a* (nm)	Crystalline phases
HT1	2.302	0.306	HT[a]
HT2	2.334	0.305	HT[a], CeO_2 fluorite
HT3	2.373	0.309	HT[a], CeO_2 fluorite
HT4	2.328	0.307	HT[a], CeO_2 fluorite

[a] Hydrotalcite phase.

Fig. 2 shows X-ray diffractograms in powder of mixed oxides. The diffractogram of solid OM1 shows the formation of solid solution NiO–MgO with periclase structure [22–26]. It has been reported that when ions Ni^{2+}, Mg^{2+} and $Al^{3+}$are coprecipitated, isomorphic substitutions of Ni^{2+} by Mg^{2+} and of Al^{3+} by Mg^{2+} are carried out which after the thermal activation, generate solid solutions due to the similar ionic size among ions [22,25]. The oxides obtained are composed of a mixture of two types of crystalline phases. In fact, the diffractograms of oxides containing cerium (OM2–OM4) indicate the formation of a solid solution NiO–MgO (periclase) and of CeO_2 (fluorite). On the other hand, the diffractograms do not have signals characterizing crystalline phases of Al_2O_3, suggesting that aluminium takes part in the crystalline network NiO–MgO due to the isomorphic substitution of Al^{3+} by Mg^{2+} given in precursor LDH.

In the case of solids obtained by coprecipitation with Ce^{3+} (OM2 and OM3), the results indicate that there was no effective inclusion of Ce^{3+} ions in the brucite-type layers of the precursor. In the solid obtained by coprecipitation with

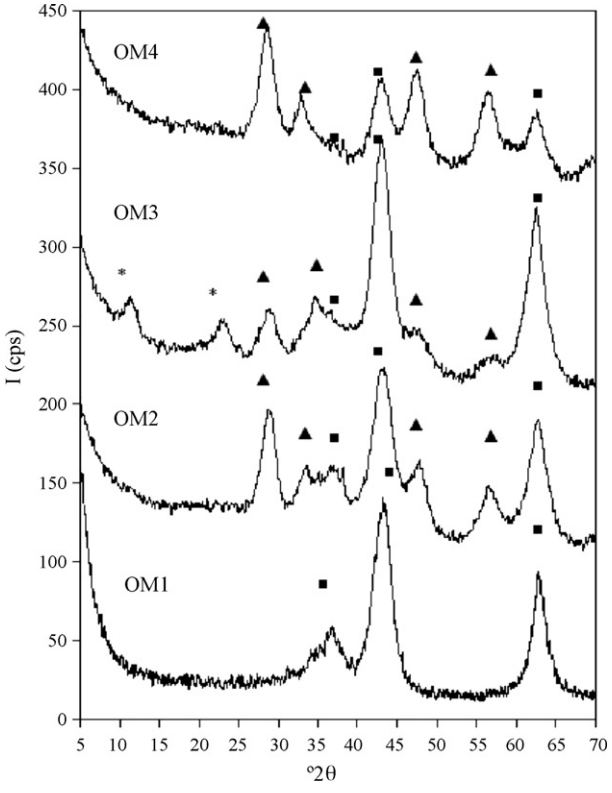

Fig. 2. XRD for the mixed oxides: (▲) CeO_2, (■) NiO–MgO periclase and (*) hydrotalcite.

$[Ce(EDTA)]^{-}$ (OM4), results suggest that after the thermal activation process, cerium could form a coating with CeO_2 particles on the starting mixed solid. In fact, some authors have pointed out that during the formation of mixed solids with $EDTA^{4-}$, the metal species included are associated to the external layers of the precursor, decorating the solid surface, as shown by XRD results, indicating that there is no increase in the crystallographic parameter *c* of precursor LDH [24]. Similarly, for the solid synthesized in the presence of $[Ni(EDTA)]^{2-}$ (OM3), the nickel would preferably be deposited, generating coatings on the surface [24].

On the other hand, it is clear that the different synthesis methods employed in this work generate oxides with different crystalline compositions. Solid OM4 is the one showing the highest content of the fluorite phase, which goes in agreement with the above results.

3.2. Thermogravimetric analysis (TGA–DTG)

Fig. 3 shows the thermogravimetric analyses for precursors of the hydrotalcite type (HT series). Each one of the precursors exhibits a two-stage thermal decomposition characterizing layered double hydroxides. The first one takes place below 200 °C and it corresponds to a weight loss from 12% to 17%. Several authors have pointed out that in this thermal event there is a loss of water, of physisorbed carbon dioxide, and the release of structural water [19,22–24,26]. We can thus appreciate that solid HT4 shows a different thermal profile from the other solids in the first temperature zone which are characterized by a more reduced weight loss. It is likely that this behaviour is due to the crystalline composition of this solid, which indicates a high CeO_2 content with respect to the carbonated hydrotalcite phase.

The second thermal event takes place between 300 °C and 400 °C and is due to the dehydroxylation of the hydrotalcite-layered structure and to the decomposition of interlayer anions [26].

The solids total weight loss ranges between 39% and 46%, and it is larger for solids synthesized in the presence of metal–EDTA complexes (OM3 and OM4). The difference is due to the decomposition of the organic ligand [26]. Likewise, a slight shift in the decomposition temperature can be observed in these solids, due to the decomposition of the metal complex, which takes place more easily than the decomposition of carbonates and nitrates. TGA–DTG results confirm the formation of the carbonated phase and the deposition of metal complexes on the external surface of the hydrotalcite.

3.3. Diffuse reflectance infrared spectroscopy (DRIFT)

Fig. 4 shows the DRIFT spectra for the HT series, confirming the typical profile of hydrotalcites. Signals between 3000 cm^{-1} and 3600 cm^{-1} correspond to –OH stretching of structural hydroxyl groups and physisorbed and interlayer water. The band at 1670 cm^{-1} is assigned to the flexion modes of water molecules. On the other hand, signals at 1420 cm^{-1} and 1050 cm^{-1} and the asymmetrical (υ_3) and symmetrical (υ_1) stretching of interlayer carbonates are shown [19,26], the latter signal appearing as a low intensity shoulder, more clearly seen in solids HT1 and HT2.

DRIFT spectra of solids HT3 and HT4 differ slightly from the DRIFT spectra of solids HT1 and HT2. It can be observed that the signals corresponding to the hydrotalcite phase show less intensity for solid HT4, which corresponds to its crystalline composition.

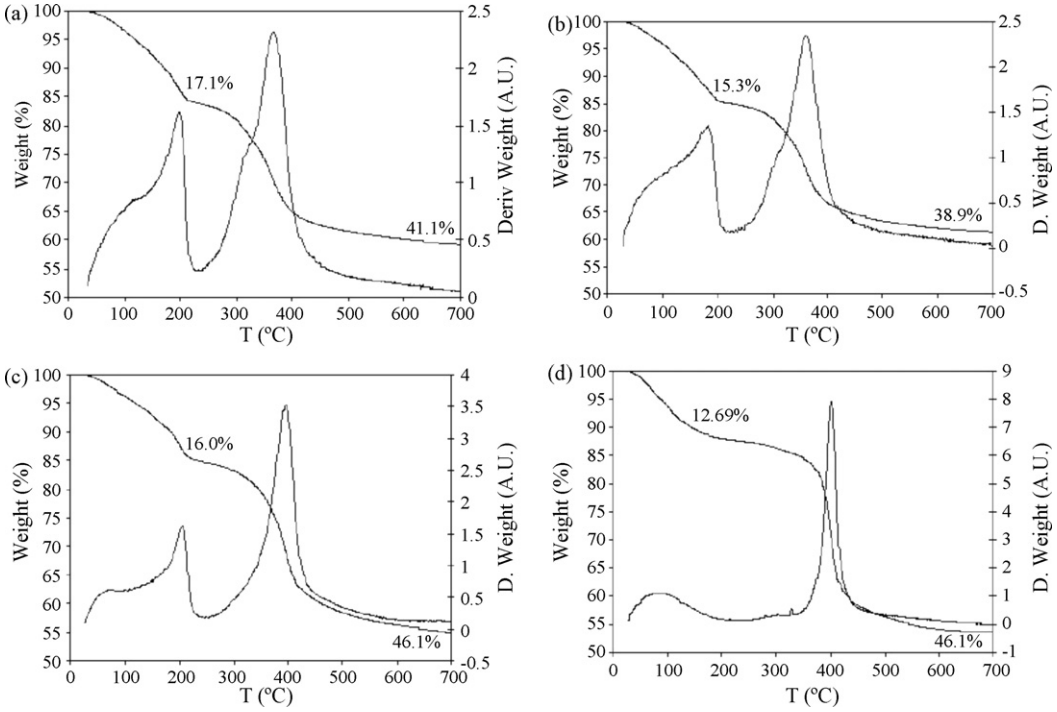

Fig. 3. TGA–DTG for the hydrotalcites: (a) HT1, (b) HT2, (c) HT3 and (d) HT4.

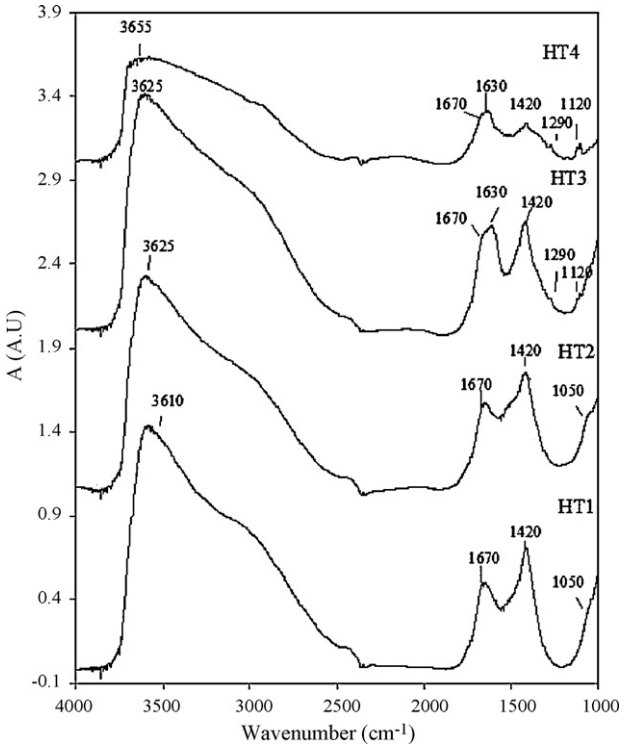

Fig. 4. DRIFT spectra for the hydrotalcites.

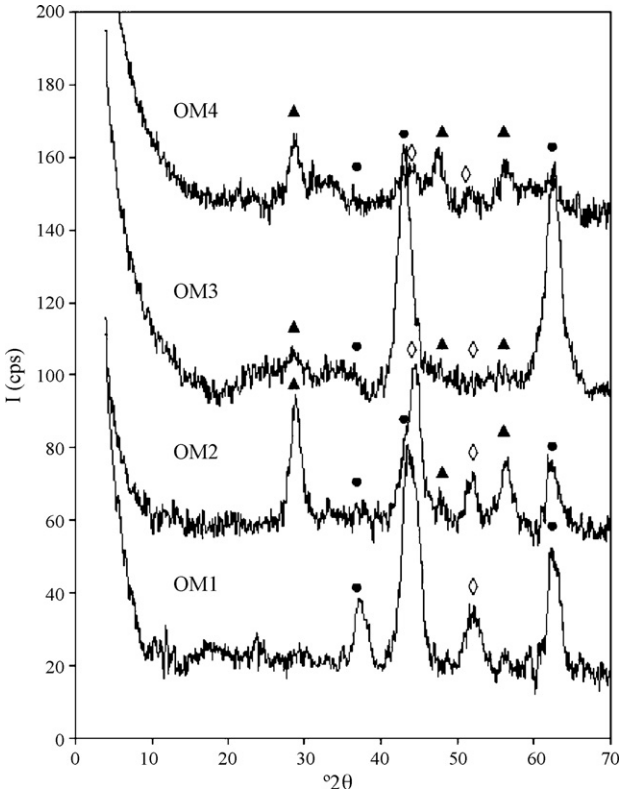

Fig. 5. XRD for the reduced catalysts (700 °C/1 h with pure H_2): (▲) CeO_2, (●) MgO periclase and (◇) Ni.

Likewise, it is possible to notice the presence of new signals corresponding to metal–EDTA complexes. Specifically, the band at 1630 cm^{-1} corresponds to COO^- group stretching, the low intensity signal at 1290 cm^{-1} corresponds to C–C stretchings, and the signal at 1120 cm^{-1} corresponds to C–N stretchings. Some authors suggest that the absence of signals above 1650 cm^{-1} indicates that the four COO^- groups are coordinated to metal ions [26]. DRIFT spectra results confirm the deposition of metal complexes on the hydrotalcite surface, which perfectly correlates with the results obtained by DRX and TGA–DTG.

3.4. XRD for the reduced mixed oxides

Fig. 5 shows the DRX patterns of reduced mixed oxides. The reduction process carried out on the solids was the same pre-treatment performed in the catalytic tests (700 °C for 1 h under pure H_2 flow at 40 mL/min). The diffractograms reveal that after the reduction process there was no formation of new crystalline phases (aluminates). Catalysts are thus composed of periclase phase containing MgO, Al_2O_3 and NiO without being reduced, fluorite-type CeO_2 and Ni that migrated to the surface to form metal crystallites [3,22,23]. Likewise, it can be observed that the pre-treatment causes some loss of crystallinity of the oxides, which is seen in the reduction in the intensity of the diffraction signals.

Table 4 records CeO_2 and Ni particle sizes calculated from the DRX results for solids reduced by means of Scherrer equation. The results show that in all cases, catalysts with Ni and CeO_2 particle sizes smaller than 10 nm are obtained. As we can observe, in some cases it was not possible to calculate the particle size due to the fact that the diffraction line is very weak and/or wide, suggesting particle size smaller than 5 nm [29]. Thus, the synthesis and activation methods used in this work produce materials with metal nanoclusters, which is particularly important in the process of CO_2 reforming of methane [2,3].

3.5. Temperature programmed reduction (TPR-H_2)

Fig. 6 shows the TPR-H_2 profiles of mixed oxides. Solid OM1 profile shows only one reduction peak with T_M at around 800–840 °C, indicating the existence of one single type of reducible species. In spite of the presence of Al^{3+} in the crystalline network, which affects stability and thus favours the reduction of Ni^{2+} [4], the strong interaction of solid solution NiO–MgO causes the reduction to take place at a high T_M as compared with the one reported for NiO (380 °C) [27]. These results agree with what has been reported by other authors [30].

Table 4
Reducibility, particle size and BET area of mixed oxides determined after reduction at 700 °C (1 h/pure H_2)

Solid	Reducibility (%)	D_p (nm)[a]		BET area ($m^2\ g^{-1}$)
		Ni	CeO_2	
OM1	86	9.5	–	265.9
OM2	92	8.0	5.5	168.1
OM3	33	NA[b]	NA[b]	106.2
OM4	83	NA[b]	6.2	33.5

[a] Determined by XRD.
[b] Not available due to very broad and weak XRD peaks.

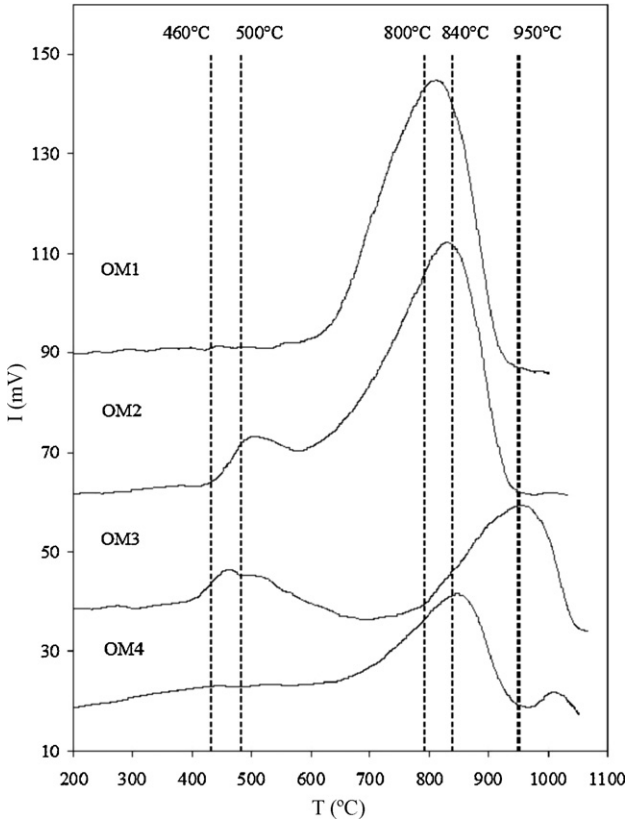

Fig. 6. TPR-H_2 for the mixed oxides.

Solid OM2 shows two reduction peaks with T_M at 500 °C and 825–840 °C, the latter having the largest intensity. The peak at 825–840 °C corresponds to the reduction of nickel in the solid solution NiO–MgO, showing a slight increase in the T_M for this process with respect to solid OM1. The reduction peak at 500 °C may correspond to two processes: (i) the reduction of the nickel not included in the coprecipitation which was deposited over segregated CeO_2, and/or (ii) the reduction of CeO_2 to Ce_2O_3, since it has been reported that the Ce(IV)/Ce(III) reduction occurs in two stages: the first one corresponding to the reduction of superficial oxygen between 480 °C and 500 °C, and the second one to the reduction of oxygen in the crystalline network between 780 °C and 800–900 °C. Our results do not allow us to explain with total certainty this reduction process [15].

Solid OM3 shows a reduction profile with two low intensity peaks with T_M at 460 °C and 500 °C and a third one at a greater intensity with a T_M of 950 °C. Species reducing at 460 °C and 500 °C may correspond to reducible species previously mentioned. On the other hand, the method for including Ni as a complexing species with $EDTA^{4-}$ using OM3 synthesis involves a low inclusion of the metal due to the low interlamellar charge characteristic of the precursors. The peak at 950 °C corresponds to the nickel reduction and it suggests that the NiO species formed by this synthesis method display higher interaction with the surface than in the case of solids OM2 and OM3. It has been reported that the metal content has an effect on the shape and T_M of the reduction peaks, and a shift towards higher reduction temperatures is noticed as the amount of metal diminishes. This is probably due to the fact that low metal contents favour the formation of smaller oxide aggregates, which therefore, show greater interaction with the surface [24,25].

Solid OM4 shows a high intensity reduction peak at 840 °C, one of intermediate intensity at 1005 °C and a slight increase in the base line between 400 °C and 500 °C, which may correspond to another reduction peak. The peak at 840 °C corresponds to the reduction of the nickel in the solid solution, and an increase is noticed with respect to the OM1 solid. Species reducing between 400 °C and 500 °C may correspond to the types mentioned for solid OM2. On the other hand, the reduction peak at 1005 °C corresponds to the reduction of lattice oxygen of CeO_2 (solid with the highest CeO_2 content) [15]. The position of this peak indicates that the synthesis methodology generates the formation of CeO_2 species with strong interaction.

Fig. 7 shows the reduction profiles (TPR-H_2) for reduced catalysts with the same pre-treatment conditions as the ones used in the catalytic tests (700 °C for 1 h under pure H_2 flow at 40 mL/min). First, results indicate that under reaction conditions, part of the nickel is not reduced. Profiles for all solids show the same peaks as the reduction profiles for not pre-treated solids; only the intensity of the peaks is reduced due to the partial reduction. Based on the profiles, it is possible to point out that lattice oxygen atoms in the CeO_2 are not reduced under pre-treatment conditions (peaks at 1000 °C in OM2 and OM4 solids).

Table 4 shows the reducibility of the catalysts. This is calculated by taking the hydrogen consumption of solids

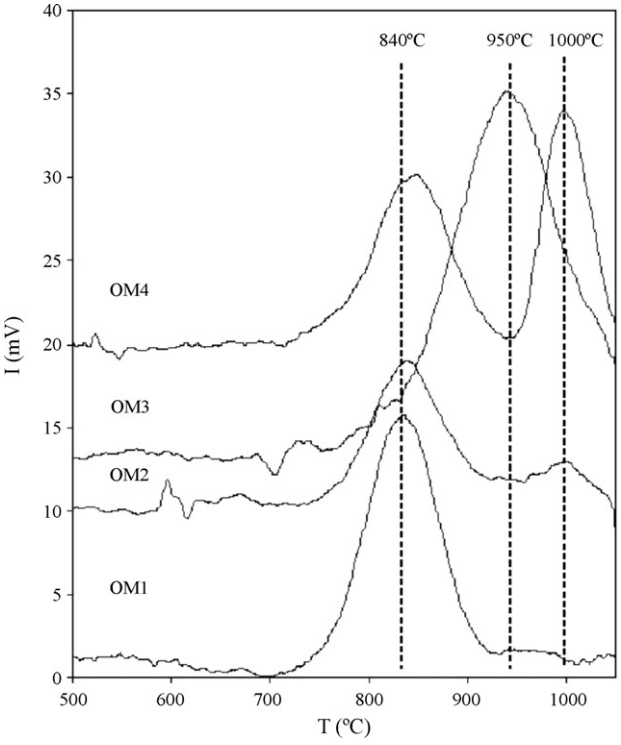

Fig. 7. TPR-H_2 for the reduced mixed oxides (700 °C/1 h, pure H_2).

with and without pre-treatment as the base. It is clear that reducibility at 700 °C depends on the maximum reduction temperature. Hence, solid OM3 shows the lowest reducibility in the synthesized series of solids. In comparison, solid OM2 shows higher reducibility than solid OM1, taking into account that the chemical composition of these two materials is the one with highest similarities, a beneficial effect of the cerium in the catalyst reduction could be suggested.

3.6. BET surface areas

Table 4 shows BET surface areas for the mixed oxides. It can be observed that in general ceria-containing solids present low surface area because CeO_2 is a non-porous material. Solid OM4 shows the lowest surface area in the synthesized series of solids due to the highest CeO_2 content and aggregate and particles sizes. On the other hand, solid OM2 presents larger surface area than solid OM3 since the last one shows Lowest CeO_2 content.

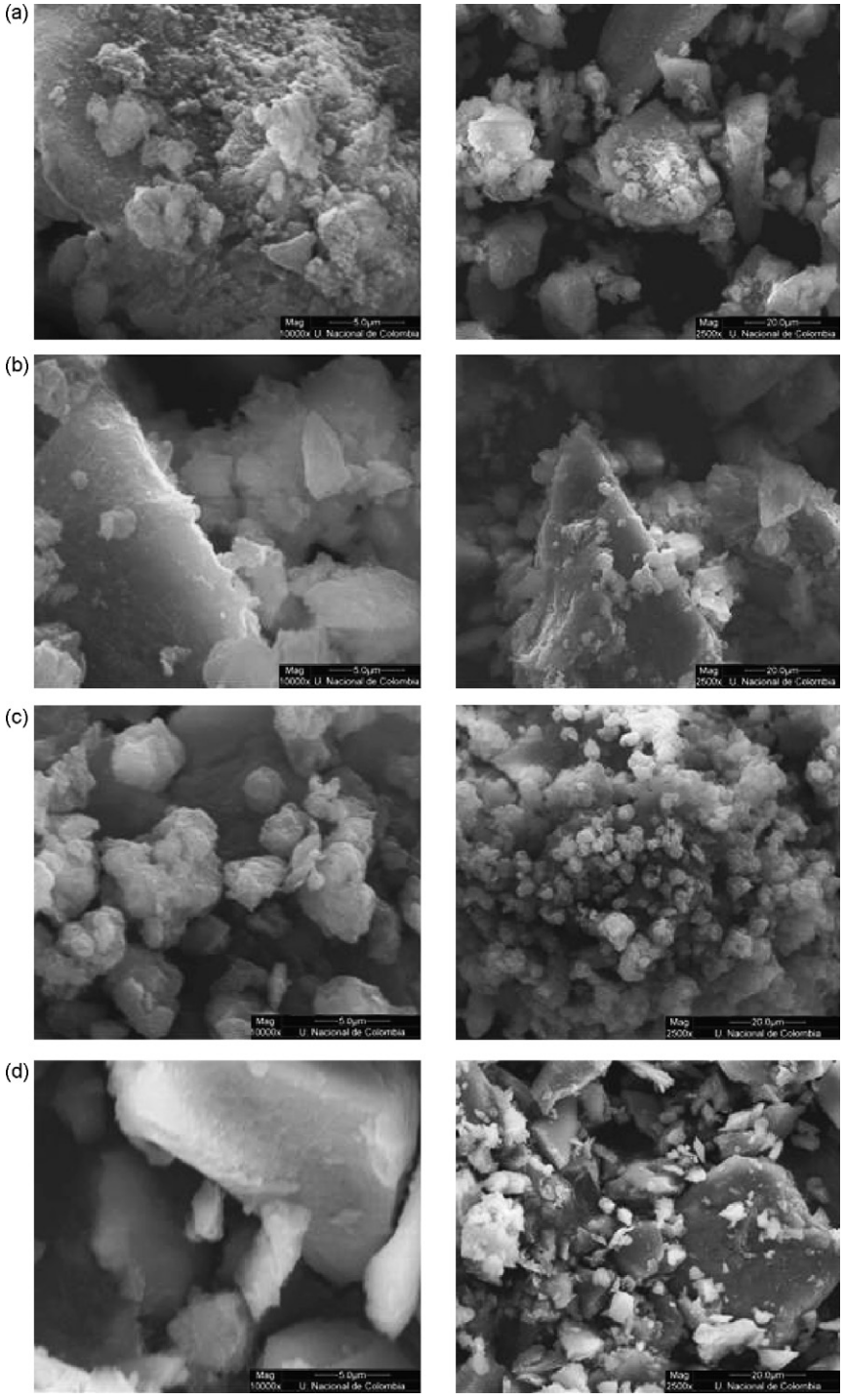

Fig. 8. SEM images for the mixed oxides: (a) OM1, (b) OM2, (c) OM3 and (d) OM4.

The coprecipitation method with metal complex leads materials with lowest surface areas.

3.7. Scanning electron microscopy (SEM-EDAX)

Fig. 8 shows SEM images for mixed solids. It can be seen that the different synthesis methods used in this work produce materials with different morphologies and grain sizes. The images taken were accompanied by a semi-quantitative EDAX analysis and chemical mapping at different resolutions, which revealed the excellent distribution of the metals making up mixes solids, suggesting a homogeneous chemical composition of aggregates.

Solid OM1 is composed of crystals with irregular shapes, well-defined corners and sizes between 5 μm and 100 μm. On some crystals, it is possible to notice aggregates of smaller sizes, probably formed during the thermal process of hydrotalcite decomposition. Solid OM2 shows a morphology, which is slightly different from solid OM1, which is composed of crystals with less defined shapes, less thickness and a wider particle size distribution. A larger number of grains of sizes smaller than 5 μm can be observed in the case of solid OM1.

On the other hand, solid OM3 is mostly composed of grains smaller than 10 μm deposited in the edges of crystalline aggregates of larger sizes. The morphology of aggregates is granular. Likewise, solid OM4 is composed of aggregates with well-defined edges and angles, and grains with larger sizes than in the case of solids OM2 and OM3.

3.8. Catalytic activity and selectivity

Fig. 9 shows the catalytic conversion of mixed oxides. In all cases, the catalytic conversion of CH_4 is lower than the one for CO_2 which indicates that probably the CO_2 is consumed in parallel in the water gas shift reaction (RWGS) [2,3]. The series of solids obtained in the presence of Ce^{3+} (OM2–OM4) shows greater catalytic activity than the solid synthesized without Ce^{3+} (OM1). Solid OM2 is the one showing higher catalytic conversion in the series. This set of results provides evidence on the promoting effect of cerium on catalytic activity.

On the other hand, solid OM3 showed the lowest catalytic activity in the series of cerium-containing solids. However, these values can be compared with those obtained for solids synthesized by coprecipitation. Solid OM3 was obtained in the presence of $[Ni(EDTA)]^{2-}$ and was the one having the smaller content of Ni^{2+} due to the limitations of including metal species by the synthesis method previously mentioned. In addition, catalytic activities of solids of the series OM2 and OM3 are stable with time under the reaction conditions used in this work.

Fig. 10 shows the selectivity catalytic of mixed oxides. Sample OM1 turned out to be more selective towards CO and sample OM2 is the most selective one towards H_2. However, selectivity values for all solids are very similar and they lie

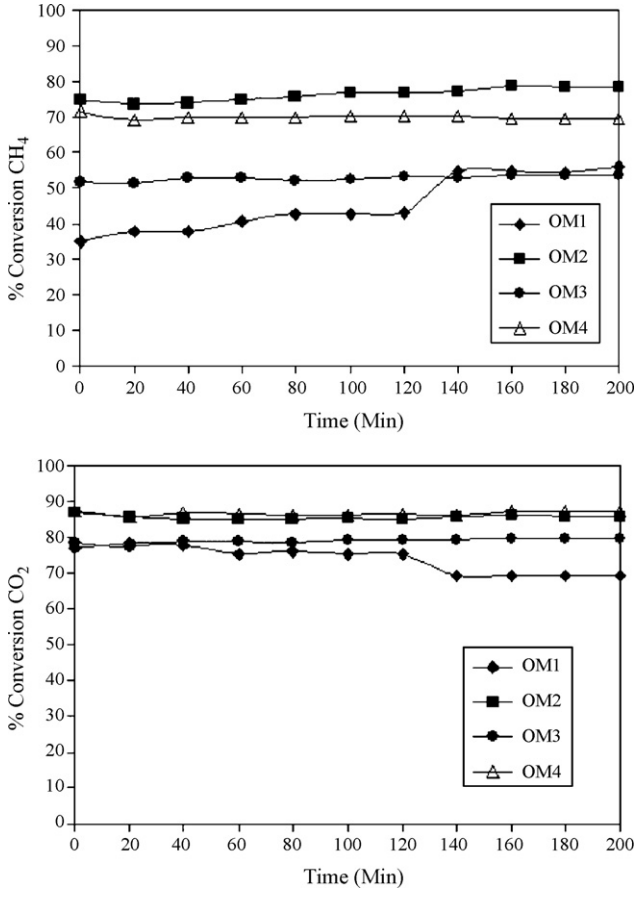

Fig. 9. Catalytic conversion vs. time for the mixed oxides.

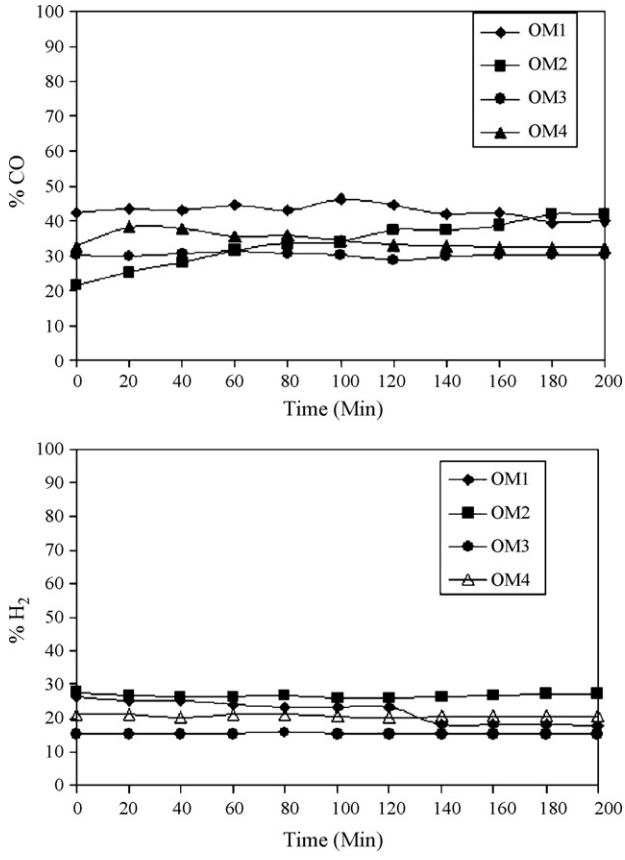

Fig. 10. Catalytic selectivity vs. time for the mixed oxides.

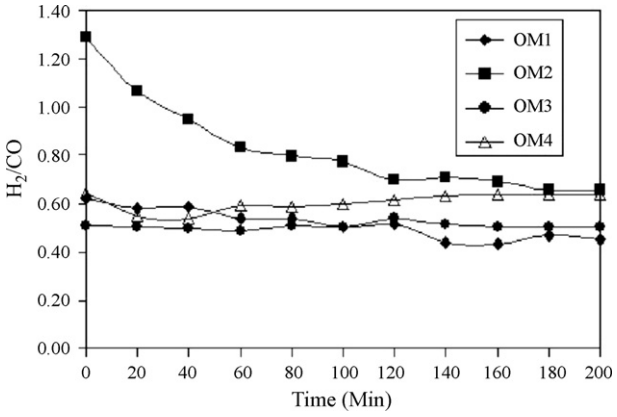

Fig. 11. H_2/CO vs. time for the mixed oxides.

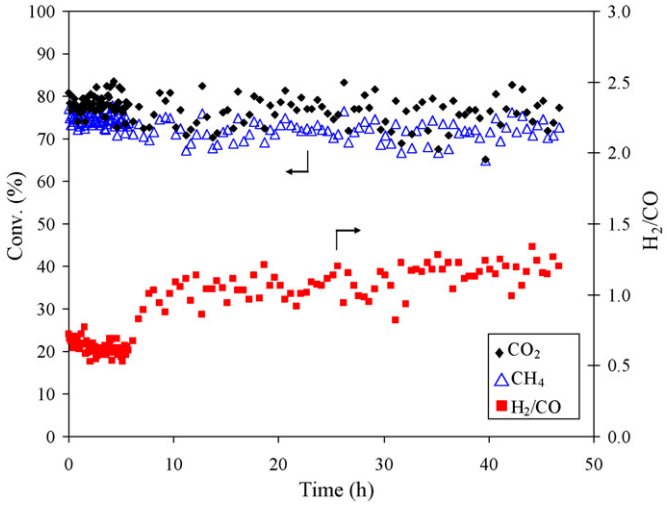

Fig. 12. Catalytic stability of the OM2 catalyst.

between 20% and 40% towards CO and 18% and 30% towards H_2, attaining stability with time.

Finally, Fig. 11 shows H_2/CO molar ratios for the synthesis gas obtained by means of synthesized catalysts in this work. We can clearly observe that molar values are always lower than 1 and higher than 0.5 due to the differences in selectivity previously mentioned. Solid OM2 is the only one in the series displaying H_2/CO values larger than 1 in the first 2 h of the reaction. However, there is a tendency to stabilize with time at values similar to those of other solids in the series. These results indicate that by using mixed solids Ni/Mg/Al/Ce, synthesis gas with proper mole ratios for further applications like the Fischer–Tropsch process can be obtained [2,3].

In order to determinate the stability of OM2 catalyst (the highest catalytic activity in the synthesized series of solids) a long time catalytic experiment was carried out. Fig. 12 shows the results. The catalyst presents an excellent catalytic stability without loss of activity until 50 h of reaction time, with CH_4 conversions of 70–80% and CO_2 conversions of 70–85%. On the other hand, the H_2/CO molar ratio is 0.5–0.8 before 7 h and 0.8–1.4 after 10 h of reaction.

4. Discussion

The results indicate that carbonated hydrotalcites are obtained by the coprecipitation methods employed. The incorporation of cerium by coprecipitation does not involve the isomorphic substitution of Ce^{3+} in the Ni^{2+}, Mg^{2+} and Al^{3+} hydrotalcite structure, due to the difference in ionic sizes. On the other hand, coprecipitation in the presence of complex anions (metal–EDTA) causes the formation of metal aggregates on the external surface of the hydrotalcite structure, which after the activation processes generate CeO_2 and Ni nanoparticles with sizes smaller than 10 nm.

It is remarkable that catalysts with low nickel contents and limited degrees of reducibility under pre-treatment conditions (OM3) display activities that can be compared with those of catalysts with considerably larger amounts of nickel (OM2 and OM4) and larger reducibility levels. This behaviour is directly related with the smaller size of the particles generated for this catalyst (<5 nm).

The increase in the catalytic activities of solids containing cerium suggests a promoting effect in this metal. In contrast, solid OM2 increases the CH_4 conversion by near 40% and that of CO_2 by about 10% by only replacing 10% of Al^{3+} by Ce^{3+} in the nominal quantities used in the synthesis. In the same way, cerium doping increases the reducibility of this catalyst as compared with OM1 without a reduction in the particle size.

The method to obtain solid OM4 is not appropriated to obtain a structured catalyst. During coprecitipation, due to excess Ce^{3+} and the preferential formation of the Ni^{2+} complex, most CeO_2 is formed, as well as a low crystallinity hydrotalcite phase. In this way, the formation of larger CeO_2 particles than those obtained with other methods is explained (6.2 nm). However, the catalytic behaviour is not related with the crystalline nature of the hydrotalcite-type precursor, but rather with the number of active sites and the size of the particle generated during the activation process. Thus, catalysts containing cerium show smaller particle sizes than solid OM1 and larger catalytic activity.

On the other hand, the stability of catalysts is related with the strong Ni-surface and Ce-surface interactions revealed by TPR-H_2 tests, which is directly linked with catalysts resistance to sinterization.

This work confirms that cerium promotes a beneficial effect on the size of nickel particles and its reducibility, and consequently, on its catalytic behaviour. For comparison purposes, other alternative synthesis methodologies to produce cerium-promoted hydrotalcites through the precipitation methods are presented.

5. Conclusions

Ni/Mg/Al/Ce mixed oxides obtained through the thermal decomposition of layered double hydroxide-type precursors synthesized by coprecipitation are promising catalysts in the reforming of methane with CO_2.

The synthesis method directs the formation of solids with crystalline compositions, different reducible species and

morphology and particle sizes smaller than 10 nm. The solids are composed of a mixture of periclase crystalline phases (NiO–MgO) and fluorite (CeO_2), indicating that there was no formation of a single composed crystalline phase for all metals used in the synthesis. The reducible species depend on the crystalline composition of the solid, but in all cases showed strong Ni-surface interactions. This information is important in the design of catalysis for the process under investigation.

Cerium has a catalytic activity promoting effect in these solids, as revealed in an increase in the conversion and stability of solids.

The catalysts obtained show high activity and good stability to produce synthesis gas with molar relations H_2/CO reaching adequate values for further applications.

Acknowledgements

This research was financed by COLCIENCIAS, Universidad Nacional de Colombia, Universidad de Antioquia (Contract 1115-06-17639), and VRI-DIB-Universidad Nacional de Colombia (20201007579).

C. Daza wishes to thank COLCIENCIAS for sponsoring his doctoral studies. F. Mondragón and J.A. Moreno wish to thank Universidad de Antioquia for the financial support of the Sostenibilidad Program.

References

[1] J.R. Rostrup-Nielsen, Catal. Today 18 (1993) 305.
[2] Y.H. Hu, E. Ruckenstein, H.K. Bruce C. Gates, Adv. Catal., Academic Press, 2004, pp. 297–345.
[3] J.R. Rostrup-Nielsen, J. Sehested, J.K. Norskov. Adv. Catal., Academic Press, 2002, pp. 65–139.
[4] C. Batiot-Dupeyrat, G.A. Sierra, F. Mondragon, J. Barrault, J.-M. Tatibouet, Catal. Today 107–108 (2005) 474.
[5] G. Sierra, F. Mondragon, J. Barrault, J.-M. Tatibouet, C. Batiot-Dupeyrat, Appl. Catal. A 311 (2006) 164.
[6] J. Guo, H. Lou, H. Zhao, D. Chai, X. Zheng, Appl. Catal. A 273 (2004) 75.
[7] G. Valderrama, M.R. Goldwasser, C.U.D. Navarro, J.M. Tatibouet, J. Barrault, C. Batiot-Dupeyrat, F. Martinez, Catal. Today 107–108 (2005) 785.
[8] S. Wang, G.Q. Lu, Appl. Catal. A 169 (1998) 271.
[9] B.-Q. Xu, J.-M. Wei, H.-Y. Wang, K.-Q. Sun, Q.-M. Zhu, Catal. Today 68 (2001) 217.
[10] L. Xiancai, W. Min, L. Zhihua, H. Fei, Appl. Catal. A 290 (2005) 81.
[11] M. Nurunnabi, B. Li, K. Kunimori, K. Suzuki, K.-i. Fujimoto, K. Tomishige, Appl. Catal. A 292 (2005) 272.
[12] M.M.V.M. Souza, M. Schmal, Appl. Catal. A 281 (2005) 19.
[13] H.Y. Wang, C.T. Au, Appl. Catal. A 155 (1997) 239.
[14] J.G. Carriazo, M.A. Centeno, J.A. Odriozola, S. Moreno, R. Molina, Appl. Catal. A 317 (2007) 120.
[15] H.C. Yao, Y.F.Y. Yao, J. Catal. 86 (1984) 254.
[16] N. Laosiripojana, W. Sutthisripok, S. Assabumrungrat, Chem. Eng. J. 112 (2005) 13.
[17] S. Wang, G.Q. Lu, Appl. Catal. B 19 (1998) 267.
[18] G. Xu, K. Shi, Y. Gao, H. Xu, Y. Wei, J. Mol. Catal. A 147 (1999) 47.
[19] V. Rives, Mater. Chem. Phys. 75 (2002) 19.
[20] A. Bhattacharyya, V.W. Chang, D.J. Schumacher, Appl. Clay Sci. 13 (1998) 317.
[21] T. Shishido, M. Sukenobu, H. Morioka, M. Kondo, Y. Wang, K. Takaki, K. Takehira, Appl. Catal. A 223 (2002) 35.
[22] A.I. Tsyganok, M. Inaba, T. Tsunoda, S. Hamakawa, K. Suzuki, T. Hayakawa, Catal. Commun. 4 (2003) 493.
[23] A.I. Tsyganok, M. Inaba, T. Tsunoda, K. Suzuki, K. Takehira, T. Hayakawa, Appl. Catal. A 275 (2004) 149.
[24] A.I. Tsyganok, M. Inaba, T. Tsunoda, K. Uchida, K. Suzuki, K. Takehira, T. Hayakawa, Appl. Catal. A 292 (2005) 328.
[25] A.I. Tsyganok, T. Tsunoda, S. Hamakawa, K. Suzuki, K. Takehira, T. Hayakawa, J. Catal. 213 (2003) 191.
[26] A. Tsyganok, A. Sayari, J. Solid State Chem. 179 (2006) 1830.
[27] R. Molina, G. Poncelet, J. Catal. 173 (1998) 257.
[28] D.A.M. Monti, A. Baiker, J. Catal. 83 (1983) 323.
[29] H.-S. Roh, H.S. Potdar, K.-W. Jun, Catal. Today 93–95 (2004) 39.
[30] K. Takehira, T. Shishido, P. Wang, T. Kosaka, K. Takaki, J. Catal. 221 (2004) 43.